

# Spectroscopic Properties of Void Galaxies in the Sloan Digital Sky Survey

Randall R. Rojas<sup>1</sup>, Michael S. Vogeley<sup>1</sup>, Fiona Hoyle<sup>1</sup>, & Jon Brinkmann<sup>2</sup>

rrojas@mercury.physics.drexel.edu, vogeley@drexel.edu, fiona.hoyle@drexel.edu

## ABSTRACT

We study the spectroscopic properties of a sample of  $10^3$  void galaxies from the Sloan Digital Sky Survey (SDSS) and compare these with the properties of galaxies in higher density regions (wall galaxies). This sample of void galaxies covers the range of absolute magnitude from  $M_r = -13.5$  to  $M_r = -22.5$  in regions with density contrast  $\delta\rho/\rho < -0.6$ . In this paper we compare the equivalent widths of  $H\alpha$ , [OII], [NII],  $H\beta$ , and [OIII] of void and wall galaxies of similar luminosities and find that void galaxies have larger values, indicating that they are still forming stars at a high rate. A comparison of the Balmer break, as measured by the parameter  $D_n(4000)$ , reveals that void galaxies have younger stellar populations than wall galaxies. Using standard techniques, we estimate  $H\alpha$  and [OII] star formation rates of the void and wall galaxies and along with estimates of the stellar masses, we compute specific star formation rates. In most cases, we find that void galaxies have similar SFRs to wall galaxies but they are fainter and smaller mass. This means that, consistent with the EWs, void galaxies have higher specific star formation rates than wall galaxies.

*Subject headings:* cosmology: observations – galaxies: large-scale structure of the universe – methods: statistical

## 1. Introduction

Studying the variation within environment of galaxy properties is fundamental to our understanding of galaxy formation and evolution. Dressler (1980) characterized the morphology-density relation – the tendency for elliptical galaxies to reside in clusters and spirals in the field. This has been subsequently confirmed by many different groups (e.g. Postman & Geller 1984; Zabludoff & Mulchaey 1998; Hashimoto & Oemler 1999; Tran et al. 2001; Dominguez et al 2001; Treu et al. 2003). Recent studies have attempted to extend the study of this environmental dependence into increasingly underdense regions. In a series of papers, we seek to examine if galaxies that reside in the most underdense regions, referred to as void galaxies, are fundamentally different from galaxies in denser environments.

---

<sup>1</sup>Department of Physics, Drexel University, 3141 Chestnut Street, Philadelphia, PA 19104

<sup>2</sup>Apache Point Observatory, P. O. Box 59, Sunspot, NM 88349-0059

Many studies have also shown that there is a strong dependence of star formation on environment. High star formation rates (SFR) are usually found in low density environments while lower SFRs are more commonly seen in higher density regions. (Dressler, Thompson & Shectman 1985; Couch & Sharples 1987; Balogh et al. 1997, 1998, 1999, 2002; Hashimoto et al. 1998; Poggianti et al. 1999; Couch et al. 2001; Solanes et al. 2001; Lewis et al. 2002a; Gomez et al. 2002).

However, only recently was it possible to show that there is a strong dependence of SFR on local galaxy density in large enough samples to include a fair mix of morphological types. Gomez et al. (2002) showed that there is a decrease in SFR from galaxies in the field to galaxies in denser environments (e.g. in rich clusters). Independently, Lewis et al. (2002a) found the same strong correlation between environment and SFRs in the 2dF Galaxy Redshift Survey. Hashimoto et al. (1998) noticed that regardless of the concentration index, galaxies in clusters have on average lower SFRs than field galaxies in the Las Campanas Redshift Survey. As well as looking at SFRs, some groups have considered the strength of  $H\alpha$  emission and consistently find that  $H\alpha$  emission has a strong dependence on local density (Balogh et al. 2004; Tanaka et al. 2003). Tremendous efforts in extrapolating the *density-sfr* relation down to lower densities have met with success. However, none have been able to probe the very lowest densities.

Void galaxies have been studied photometrically by Grogin & Geller (1999) and by Rojas et al. (2004). They demonstrated that there are significant differences between void and non-void galaxies, with void galaxies being bluer in color and having morphologies that more closely represented late-type galaxies. However, they found that this was not just an extension of the morphology-density relation as late-type galaxies in low density environments were bluer than late-type galaxies in higher density environments and the same held for early-type galaxies i.e. density plays a role in the properties of the same type of galaxies rather than just changing the relative mix of type of galaxy.

In this paper, we focus on the spectroscopic properties of void galaxies to examine the role of density on the strength of the equivalent widths of various lines and on star formation rates. Using a sample of 150 galaxies with  $\delta\rho/\rho < 0$ , Grogin & Geller (2000) showed that the  $EW(H\alpha)$ -density relation is most noticeable in either the lowest or highest density environments i.e the void galaxies had large  $EW(H\alpha)$  and the galaxies in richer environments had smaller values of  $EW(H\alpha)$ . We extend this work by using a sample of  $10^3$  void galaxies with density contrast  $\delta\rho/\rho < -0.6$  that spans a broad range of absolute magnitude from  $M_r = -13.5$  to  $M_r = -22.5$ . We use this sample to quantitatively extend the study of star formation history down to the lowest densities possible and compare the spectroscopic properties of our void galaxies with non-void galaxies of similar luminosities and surface brightness profiles. These comparisons are crucial in order to constrain models of galaxy formation and evolution.

In Section 2 we discuss the data sample. In Section 3 and 4 we present the results of the various spectroscopic parameters. We compare the results with those from other groups in Section 5. Finally, in Section 6 we present our conclusions.

## 2. The Data

We identify a sample of  $10^3$  void galaxies from early data available from the SDSS. The SDSS is a wide-field photometric and spectroscopic survey that will cover approximately  $10^4$  square degrees. CCD imaging of  $10^8$  galaxies in five colors and follow-up spectroscopy of  $10^6$  galaxies with  $r < 17.77$  will be obtained. York et al. (2000) provides an overview of the SDSS and Stoughton et al. (2002) describes the early data release (EDR) and details about the photometric and spectroscopic measurements and Abazajian et al. (2003, 2004) describe the first (DR1) and second (DR2) data releases. Technical articles providing details of the SDSS include descriptions of the photometric camera (Gunn et al. 1998), photometric analysis (Lupton et al. 2002), the photometric system (Fukugita et al. 1996; Smith et al. 2002), the photometric monitor (Hogg et al. 2001), astrometric calibration (Pier et al. 2003), selection of the galaxy spectroscopic samples (Strauss et al. 2002; Eisenstein et al. 2001), and spectroscopic tiling (Blanton et al. 2003a). A thorough analysis of possible systematic uncertainties in the galaxy samples is described in Scranton et al. (2002). All the galaxies are k-corrected according to Blanton et al. (2003b) and we assume a  $\Omega_m, \Omega_\Lambda = 0.3, 0.7$  cosmology and Hubble’s constant,  $h = H_o/100 \text{ km s}^{-1}\text{Mpc}^{-1}$  throughout.

In this paper, we consider the spectral properties of galaxies in different environments. The SDSS spectra cover the wavelength range 3900-9100Å, obtained using a double blue/red spectrograph with the beam split at 6150Å by a dichroic. The data have spectral resolution ranging from 1800 to 2100 (i.e.  $\lambda/\delta\lambda \approx 2000$ ), so at 4000Å the resolution is  $\sim 2\text{Å}$ . The signal-to-noise ratio, S/N, is typically 13 per pixel.

Void galaxies are drawn from a sample referred to as **sample10** (Blanton et al. 2002). This sample covers nearly  $2000 \text{ deg}^2$  and contains 155,126 galaxies. We use a nearest neighbor analysis, described in more detail below, to find galaxies that reside in region of density contrast  $\delta\rho/\rho < -0.6$  as measured on a scale of  $7h^{-1}\text{Mpc}$ , which we label void galaxies. Galaxies with larger values of  $\delta\rho/\rho$  are referred to as wall galaxies. Full details of void galaxy selection are described in Rojas et al. (2004). Here we provide a brief overview, as follows. First, a volume-limited sample of relatively bright galaxies is constructed to define the density field that traces the distribution of voids. This volume-limited sample extends to maximum redshift  $z_{\text{max}} = 0.089$ . We identify void galaxies from the flux limited sample, also truncated at  $z = 0.089$ . We discard galaxies that lie close to the edge of the survey, because it is impossible to tell if a galaxy is a void galaxy if its neighbors could not yet have been observed. For each of the remaining galaxies in the flux-limited sample, we measure the distance to third nearest neighbor the volume-limited catalog. A galaxy with fewer than three neighbors within a sphere of radius  $7h^{-1}\text{Mpc}$  is flagged as a void galaxy. Galaxies with more than 3 neighbors we label as wall galaxies. This procedure yields a sample of 1,010 void galaxies and 12,732 wall galaxies. These void and wall galaxies span a redshift range  $0.034 \lesssim z < 0.089$  and a range of absolute magnitudes from  $-22 < M_r < -17.77$ . This sample is referred to as the “distant” sample. This sample is also split in absolute magnitude at  $M_r = -19.5$  into bright [WGD\_b, VGD\_b] ( $M_r \leq -19.5$ , b=bright, W=wall, V=void) and faint [WGD\_f, VGD\_f] ( $M_r > -19.5$ , f=faint) sub-samples respectively.

We construct a sample of fainter and more nearby void galaxies – the “nearby” sample – by using the wider angle Updated Zwicky Catalog (Falco et al. 1999) and the Southern Sky Redshift Survey (da Costa et al. 1998) to trace the distribution of local voids (see figure 1. in Rojas et al. 2004), at distances where the slices of available SDSS scans (which extend over roughly 2.5 degrees in declination) are too narrow to accurately map the large-scale structure. We construct volume-limited samples of the UZC and SSRS2 to match the density of objects used as tracers for the “distant” sample of SDSS galaxies. These nearby samples extend to maximum redshift  $z_{\text{max}} = 0.025$ . We apply the same nearest neighbor analysis and identify a further 194 void galaxies and 2,256 wall galaxies from a flux-limited sample of SDSS galaxies. The absolute magnitudes of these galaxies lie in the range  $-19.7 < M_r < -13$ . We also split the Nearby sample into bright [WGN\_b, VGN\_b] ( $M_r \leq -17$ , b=bright) and faint [WGN\_f, VGN\_f] ( $M_r > -17$ , f=faint) subsamples.

### 3. Measured Spectroscopic Properties

In this paper we study the spectroscopic differences between void and wall galaxies. We compare their  $H\alpha$ , [OII]  $\lambda 3727$ ,  $H\beta$ , [NII]  $\lambda 6583$ , [OIII]  $\lambda 5007$  equivalent widths (EWs), stellar masses, 4000 Å Balmer break (ratio of the average flux density in the bands 4050-4250 and 3750-3950 Å,  $D_n(4000)$ ; Bruzual 1983).

We choose these quantities to examine a broad range of features in the spectra of our galaxies and star formation on different time scales. For example, the  $H\alpha$  line probes star formation on timescales of  $\sim 10^7$  years (lifetime of an HII region) whereas the 4000 Å break probes timescales of  $t \sim 1$  Gyr.

These emission lines are sensitive to a range of properties of star formation regions.  $EW(H\alpha)$  measures the ratio of flux from recent star formation (mainly flux from UV photons i.e.,  $\lambda < 912$  Å) to the integrated past star formation (predominantly flux from old stellar populations) whereas the [OII] forbidden line is due to UV radiation ( $\lambda < 730$  Å) produced by massive stars that ionize heavier elements. The [OII] line’s dependence on excitation and oxygen abundance makes it a somewhat less reliable measure of current star formation (Koo and Kron 1992). Note that [OII] cannot be detected in 90% of the nearby galaxies because it can only be measured by the SDSS at a redshift of  $z \approx 0.07$ . No [OII] results are given for the nearby sample.

$EW(H\alpha)$  is typically double that of [OII] but the [OII] line is less affected by dust than  $H\alpha$ . In both cases, large values of EW suggest high star formation. Large  $H\alpha$  equivalent widths are directly related to high star formation rates, bluer colors and fainter absolute magnitudes (Kennicutt & Kent 1983). Strong correlations between  $EW([OII])$  and galaxy colors have been shown to exist for various galaxy types and redshifts (Huchra 1977; Peterson et al. 1986; Broadhurst, Ellis, & Shanks 1988; Colless et al. 1990; Broadhurst, Ellis, & Glazebrook 1992; Koo & Kron 1992).

We use the widths of the Gaussian fit to the respective lines as measured by the SDSS spectral

pipeline (`spectro1d`; SubbaRao et al, 2004). For the 4000 Å break strength we use, where possible, Kauffmann et al’s. (2003; K03) estimates of this index ( $D_n(4000)$ ). They use the ratio of the average flux density in narrow continuum bands (3850-3950 and 4000-4100 Å) as suggested by Balogh et al. (1999).  $D_n(4000)$  is an excellent indicator of past star formation on timescales of  $t \sim 1\text{Gyr}$  and is also insensitive to dust attenuation. For hot stars where elements are multiply ionized the opacity decreases. Therefore, hot, young stars (e.g., O and B) have lower amplitudes of  $D_n(4000)$  than cooler, older stars (e.g., K and M; see Figure 3, Bruzual 1983). Since late-type galaxies are mainly composed of young stars, their 4000 Å break is smaller than for early-type galaxies which are primarily composed of older stellar populations.

We compute the means and the errors on the mean of the distributions of EW’s and  $D_n(4000)$ ’s of void and wall galaxies. We also use the *Kolmogorov-Smirnov* (KS) test to examine whether the void and wall galaxies could be drawn from the same parent population based on the spectroscopic properties under consideration.

Tables 1 and 2 summarize the results of these tests for the nearby and distant samples respectively. We present results for the whole sample, as well as the samples split by absolute magnitude. The results are considered in detail below.

### 3.1. Equivalent Widths

In Tables 1 and 2 all the values of the EW of the different lines ( $H\alpha$ , [OII] (where possible),  $H\beta$ , [NII] and [OIII]) and samples (distant, nearby, bright, faint) are given. In Figures 1 and 2 we show normalized histograms of  $EW(H\alpha)$  and  $EW([OII])$  for the different samples. The solid lines correspond to the void galaxies and the dotted lines to the wall galaxies.

Void galaxies have average  $EW(H\alpha)$  of  $19.14 \pm 0.68$  in the distant sample whereas wall galaxies have  $EW(H\alpha) = 11.77 \pm 0.16$ . The quoted errors are the error on the means and these will be quoted throughout. In the nearby sample, the values are higher,  $EW(H\alpha) = 35.31 \pm 0.26$  (void) and  $26.18 \pm 0.65$  (wall). The values for  $EW([OII])$  in the distant sample are  $14.26 \pm 0.40$  (void) and  $9.44 \pm 0.09$  (wall). In all the distant samples, we find that void galaxies have on average larger EWs than wall galaxies with differences in the means  $> 5\sigma_\mu$ . In the nearby samples, the differences are around  $2\sigma_\mu$  due to the smaller sample size.

The statistical significance of the  $EW(H\alpha)$  differences between void and wall galaxies is quantified through a KS test. For the distant samples it is very unlikely that the void and wall galaxies are drawn from the same parent population ( $P < 10^{-4}$ ). In the case of the nearby samples only the faint sub-sample shows a larger probability ( $P = 0.37$ ) of being drawn from the same parent population. We attribute this in part to the decrease in number of galaxies in this sample.

A further test that we do is to split the distant galaxies by morphology. Galaxies with Sérsic index  $< 1.8$  have surface brightness profiles that resemble spirals, where as galaxies with Sérsic

index  $> 1.8$  are more like ellipticals (see Rojas et al. 2004 for the justification). In these cases, void galaxies also have statistically significant larger EWs.

### 3.2. $D_n(4000)$

From Tables 1 and 2 we can see that there is a very low probability ( $P < 10^{-4}$ ) that the distributions of  $D_n(4000)$  of void and wall galaxies (Distant and Nearby) are drawn from the same parent population.

In Figure 3 we show the distributions of  $D_n(4000)$  for the void and wall galaxy samples. We can observe two noticeable features: (1) all samples of void galaxies have on average smaller  $D_n(4000)$  than wall galaxies and (2) there is an obvious deficit of early-type galaxies in the nearby samples which is observed in the amplitude of the distributions for  $D_n(4000) \gtrsim 1.5$ . This is consistent with the results of Rojas et al. (2004), where there were few galaxies with Sérsic and concentration indices typical of early-type galaxies. The lower values of  $D_n(4000)$  indicate that there is more recent star formation in the void galaxies.

## 4. Derived Spectroscopic Properties

An alternative way of comparing the spectral properties of void and wall galaxies is to convert the spectral lines into estimated star formation rates (SFR). This is discussed below in section 4.2. We also wish to compute the *specific* star formation rate, i.e. the SFR divided by the mass of the galaxy. For this, we obviously require masses and we discuss this first.

### 4.1. Stellar Masses

The integrated stellar masses for our 70% of our sample come from K03’s library of stellar masses. They estimate the stellar masses by taking the product of the model predicted  $z$ -band stellar-mass-to-light ratio  $(M/L)_z$  and the respective dust-corrected luminosity of the galaxy. The model used by K03 to predict the  $(M/L)_z$  and stellar masses is based on median likelihood estimates from their library of Monte Carlo realizations of different star formation histories. 30% of the galaxies are missing from K03 as they took galaxies from DR1 (Abazajian 2003) where as our sample is from a larger database (Blanton et al. 2002; `sample10`). For these galaxies, we use the  $z$ -band absolute magnitude to estimate the mass as there is a nearly linear relationship between this and the logarithm of the estimated stellar mass in K03. This relationship is shown in Figure 4. We can see that the scatter is well restricted to a narrow range about the line of best fit ( $\text{Log}_{10}(\text{mass}/M_{\odot}) = -0.5134M_z - 0.01581$ ). Using this fit we estimate we can measure typical stellar masses to within a factor of 5.

In Figure 5 we show the normalized histograms of the masses for all the samples. The differences between these distributions are listed in Tables 1 and 2. It can be readily seen in the distant sample that on average void galaxies have smaller stellar masses than wall galaxies ( $10^{10.13 \pm 0.02} M_{\odot}$  as opposed to  $10^{10.43} M_{\odot}$ ). The KS test shows that it is very unlikely that void galaxies are drawn from the same parent population ( $P < 10^{-4}$ ). However, in the nearby samples the mean values of the void and wall galaxy masses are more similar ( $10^{8.69 \pm 0.06} M_{\odot}$  and  $10^{8.80} M_{\odot}$ ).

#### 4.2. Star Formation Rates

In order to calculate SFR, the basic steps are 1.) measure the flux in each line, 2.) convert the flux into a luminosity and 3.) use Kennicutt’s (1998) formulas for SFRs. Each of these steps is more involved than it sounds. In general, we employ the SDSS SFR prescription of Hopkins et al. (2003) with minor variations as discussed below. We calculate the SFR for H $\alpha$  and [OII].

The flux is obtained via

$$F = \sqrt{2\pi}\sigma\kappa \times 10^{-17} [\text{erg cm}^{-2} \text{ s}^{-1}] \quad (1)$$

where  $\sigma$  and  $\kappa$  are the widths and heights of the Gaussian fit to the respective line. These come from the SDSS spectroscopic data analysis pipeline.  $\kappa$  is in units of  $[\text{erg cm}^{-2} \text{ s}^{-1} \text{ \AA}]$  and  $\sigma$  in units of  $[\text{\AA}]$ .

The next step is to compute the respective luminosity ( $L$ ) using:

$$L = 4\pi D_L^2 F [\text{erg s}^{-1}] \quad (2)$$

where  $D_L$  is the luminosity distance in units of  $[\text{cm}]$ .

Finally, using Kennicutt’s (1998b) formula for the H $\alpha$  flux valid in the Case B recombination (Osterbrock 1986) with a Salpeter (1955) initial mass function, we compute the SFR using

$$\text{SFR} = 7.9 \times 10^{-42} L [M_{\odot} \text{ yr}^{-1}]. \quad (3)$$

and for [OII] we use Kennicutt’s (1998) calibration

$$\text{SFR} = 1.4 \times 10^{-41} L [M_{\odot} \text{ yr}^{-1}]. \quad (4)$$

However, each of these steps is more complicated than it seems as there are several corrections that must be accounted for. These include stellar absorption corrections, aperture effects, dust and smearing. We discuss each of these below.

Following Hopkins et al. (2003) we begin by applying the stellar absorption correction. This consists of correcting the observed Balmer line equivalent width (EW) by a factor ( $\text{EW}_c$ ) appropriate for the type of galaxy being studied. Hopkins et al. (2003) adopt a value of  $\text{EW}_c = 1.3 \text{ \AA}$

for their analysis of the SDSS DR1 (Abazajian et al. 2003) sample. Miller & Owen (2002) found that this correction varies from  $0.9\text{\AA}$  (E type) to  $4.1\text{\AA}$  (extreme spirals). In our case a correction of  $\text{EW}_c = 1.4\text{\AA}$  is more appropriate for the morphological mix of our galaxies (C. Tremonti private communication). This correction is then converted to a flux correction via  $F_c = \frac{\text{EW} + \text{EW}_c}{\text{EW}} F$ , where  $F$  is the observed line flux (Equation 1) and  $F_c$  the corrected line flux.

The next step is to correct the stellar absorption corrected flux  $F_c$  for aperture effects. Because emission detected through the  $3''$  fiber from a galaxy depends greatly on the redshift of the galaxy (nearby a smaller area of the galaxy is detected and at greater distances a larger area can be detected) we need to estimate the flux that would be measured in the  $3''$  fiber. This is accomplished by scaling  $F_c$  by  $10^{0.4(M_{r(\text{spec})} - M_{r(\text{petro})})}$  where  $M_{r(\text{spec})}$  and  $M_{r(\text{petro})}$  are the synthetic and Petrosian<sup>1</sup> k-corrected SDSS  $r$ -band absolute magnitudes respectively. Therefore, the stellar absorption and aperture corrected flux ( $F'_c$ ) is

$$F'_c = F_c \times 10^{0.4(M_{r(\text{spec})} - M_{r(\text{petro})})} [\text{erg s}^{-1}]. \quad (5)$$

By far the largest correction (about a factor of 10 consists of accounting for obscuration by dust. Here we apply the Fitzpatrick (1998) parameterization and compute the color excess  $E(\text{B-V})$  from the Balmer decrement given by  $\tau_{\text{Balmer}} = \ln[\frac{F'_c(H\alpha)}{F'_c(H\beta)}] / 2.87$  where  $F'_c(H\alpha)$  and  $F'_c(H\beta)$  are the stellar absorption and aperture corrected  $H\alpha$  and  $H\beta$  fluxes respectively and:

$$E(\text{B} - \text{V}) = 1.086 \tau_{\text{Balmer}} / 1.17. \quad (6)$$

Significant underestimates of the derived SFRs would be expected if this effect were unaccounted for. In the case of SFRs derived from the  $[\text{OII}]$  line, the situation is even more severe because of the larger variation of  $\tau_{\text{Balmer}}$  (Gallagher et al. 1989; Kennicutt 1992a). This implies that SFRs of ‘dustier’ galaxies will have considerably larger corrections (increase in flux) than dust poor galaxies. We find that void galaxies are relatively dust poor and therefore, wall galaxies have the largest increase in flux due to reddening corrections. This corrections are quite significant: wall galaxies have an average factor of 13 increase in flux vs. void galaxies which have a factor of 9 increase after all the relevant corrections are applied.

Note that for  $F'_c(H\beta)$  we use the  $g$ -band absolute magnitude when estimating the aperture corrections. For all other fluxes the  $r$ -band is used. With an estimate of the color excess for each galaxy we can now de-redden the  $H\alpha$ ,  $H\beta$  and  $[\text{OII}]$  fluxes using the  $R$ -dependent Galactic extinction curve of Fitzpatrick & Massa (1999). The dust corrected  $F'_c$  is now substituted into Equation 2. to compute the respective absorption, aperture, and dust corrected luminosity from which the SFR is derived using Equation 3.

---

<sup>1</sup>The magnitudes that are measured from the SDSS are Petrosian magnitudes (Petrosian 1976). The Petrosian magnitude is the total amount of flux within a circular aperture whose radius depends on the shape of the galaxy light profile, i.e., the size of the aperture is not fixed so galaxies of the same type are observed out to the same physical distance at all redshifts. More details are given in Stoughton et al. (2002).



Our analysis also accounts for smearing in the SDSS spectroscopic observing procedure (Stoughton et al. 2002). It consists of four minute spectroscopic observations performed while the telescope dithers for the purpose of correcting for light losses from the  $3''$  fiber aperture. For galaxies about  $1/3$  of their light is contained within the  $3''$  fiber aperture. Although the systematic differences between smear corrected and original spectra are only about 10% (Hopkins et al. 2003) the increase in the reported flux is generally about a factor of 2. Fortunately this was accounted for by using the  $r$ -band Petrosian magnitude in the aperture correction factor (this essentially scales the spectrum to match the photometry which is more reliable). An inherent assumption is that the  $\text{EW}(\text{H}\alpha)$  and reddening are constant across the whole galaxy.

In Tables 1 and 2 we summarize the results from the SFR estimates and compare the SFR normalized distributions for void and wall galaxies in Figures 6 ( $\text{SFR}(\text{H}\alpha)$ ) and 7 ( $\text{SFR}([\text{OII}])$ ). As noted above,  $\text{SFR}([\text{OII}])$  can only be determined from the distant sample as  $[\text{OII}]$  does not appear in the spectra of most of the nearby sample of galaxies.

In the distant sample, the wall galaxies have slightly higher SFR than the void galaxies ( $0.747 \pm 0.007 M_{\odot}/\text{yr}$  vs.  $0.734 \pm 0.025 M_{\odot}/\text{yr}$  for  $\text{H}\alpha$  and  $0.488 \pm 0.006 M_{\odot}/\text{yr}$  vs.  $0.448 \pm 0.015 M_{\odot}/\text{yr}$  for  $[\text{OII}]$ ). However, in the nearby sample, the void galaxies have slightly higher SFR than the wall galaxies. Note carefully that comparing SFRs is a little misleading though as the void galaxies are known to be fainter than the wall galaxies and have smaller masses (section 4.1) and thus would not be expected to have as high SFRs. A fairer comparison is to use the specific star formation rate, which we discuss below.

Note that when computing the means, errors on the means, and the KS statistic we include the negative SFRs in all the calculations. Negative SFRs are obtained when either emission lines are seen as absorption lines or when the strength of the line is too weak and therefore, dominated by noise. The only SFRs that are not included are those for which an estimate of the color excess was not possible because  $F'_c(\text{H}\alpha)/F'_c(\text{H}\beta) < 0$ . Our samples of void and wall galaxies are reduced by about 12% due to this restriction.

### 4.3. Specific Star Formation Rates

The SFR per unit stellar mass (S-SFR) is perhaps a more informative spectral indicator for our purposes because void galaxies are on average less luminous and have smaller stellar masses. We estimate the S-SFRs using the stellar masses and the absorption, aperture, and dust corrected SFRs as discussed above. Note that as above, we have the same caveat in our calculations, namely that the dust correction is a large effect. Consistent with our analysis of the SFRs, we include negative S-SFRs in the calculation of the mean. Neither the negative SFRs or negative S-SFR have a physical meaning, yet if we remove the 11% of galaxies that have  $\text{S-SFR} < 0$  the results would have an artificial shift in the S-SFR distributions.

In Figures 8 and 9 we show the S-SFR distributions for the  $\text{H}\alpha$  and  $[\text{OII}]$  lines respectively.

In the distant samples (bright and faint), including sub-samples split by Sérsic index, void galaxies have larger average S-SFRs( $H\alpha$ ) and S-SFRs([OII]) than wall galaxies. The KS test shows that the probability of void and wall galaxies being derived from the same parent population is  $< 10^{-4}$ . Thus, consistent with the results from the EWs, void galaxies are forming more stars per unit mass than the wall galaxies.

An apparent exception to this picture is that wall galaxies in the faint nearby sample have higher SFRs and SSFRs than the void galaxies. However, the EWs are the other way round; void galaxies have stronger equivalent widths, although the differences are within  $1-2\sigma$ . The photometric properties of these galaxies are also least distinct, the void galaxies are slightly bluer but the morphological properties are very similar (Rojas et al. 2004). It is quite possible that the dust corrections applied to obtain the SFR are not applicable for this class of faint,  $M_r < -17$ , galaxies or it is possible that the wall galaxies in this category are also somewhat isolated. A detailed study of the individual galaxies and/or a larger sample that can be more finely split as a function of density is required to study this ground of galaxies in more detail.

## 5. Discussion

To recap, we find that in all cases, distant or nearby, bright or faint, that the void galaxies have higher EWs than galaxies that reside in higher density regions. In most cases void galaxies also have higher SSFRs than wall galaxies. In any case, equivalent width measurements are less affected by the large uncertainties than the SFR and SSFR calculations and, as such, are a more reliable indicator of the recent star formation histories of galaxies. In this section, we see if these results are consistent with work from other groups.

The role of a galaxy’s environment on star formation has long been studied. Recent work has tended to focus on galaxies in environments that are more dense than the void galaxy sample that we present here. The exception is the work of Grogin and Geller (2000), who probed the SFR-density relation using a sample of 150 galaxies with values of  $n/\bar{n} < 1$ , i.e.  $\delta\rho/\rho < 0$ . 46 of these galaxies had  $\delta\rho/\rho < -0.5$ . They found that the strength of EW( $H\alpha$ ) was  $2-3\sigma$  stronger than that of galaxies at higher environments, consistent with our results. We are able to probe to even lower density environments and find that the trend continues even more strongly.

Balogh et al. (2004) also studied the strength of EW( $H\alpha$ ) in a different range of environments, from groups to low density regions. They consider both projected and three-dimensional density estimates, the latter on scales of  $1.1h^{-1}\text{Mpc}$ . They also find that the strength of EW( $H\alpha$ ) increases as density decreases. They find that rather than the whole population increasing in  $H\alpha$ , it is the fraction of galaxies that show measurable  $H\alpha$  that dominates this increase. Even so, in their most underdense environments, 30% of the galaxies still show very little, EW( $H\alpha < 4$ ), emission. We find that 12-18% of the void galaxies have very little  $H\alpha$  emission. They also consider the density on scales of  $5.5h^{-1}\text{Mpc}$  but due to a smaller data set, they examined the SDSS EDR, the results

were limited. They suggested that on these larger scales, the difference between  $\text{EW}(\text{H}\alpha)$  in void and wall regions might be greater, consistent with our results.

Gómez et al. (2003) go one step further and calculate SFRs and SSFRs as a function of density. They use a projected density estimate so a 1-1 comparison is difficult and they do not probe environments that are quite as underdense as those in this study. For example, the strongest  $\text{H}\alpha$  emitting galaxies have  $\text{EW}(\text{H}\alpha)$  of 19, which is the average value for our void sample. Nevertheless, they also find that SFR increases as the project density decreases, although there is a large scatter. Lewis et al. (2004) perform a similar analysis using the 2 degree Field Galaxy Redshift Survey and find very similar results. Gómez et al also examine whether the morphology density relation is the reason for this change in star formation. They find that late-type galaxies, as classified by the concentration index, have stronger SFR in lower density environments than in high density environments, consistent with our findings and results from Hashimoto et al. (1998), Couch et al. (2001), and Pimbblet et al. (2001). Kauffmann et al. (2004) also probe SFR as a function of density, although their lowest density bin includes more than 20% of galaxies, where as the void galaxy sample here includes only the lowest 5-8% of galaxies. The see similar trends of SFR with density, high star formation in the lowest density regions, but in contrast to Balogh et al. (2004) and the results here, they claim that the trend in SFR only occurs on small,  $< 2h^{-1}\text{Mpc}$ , scales.

The observed photometric and spectroscopic properties of void galaxies generally agree with predictions from semi-analytic models of structure formation (Benson et al. 2003) and scenarios where galaxy-galaxy interactions govern galaxy evolution. These models attempt to include feed-back effects from star formation. Void galaxies modeled in this fashion are bluer, more disk-like, and have higher specific star-formation rates than objects in denser regions. Benson et al. (2003) find that the differences between void and wall galaxies in their simulations are due to the shift toward smaller mass of the halo mass function in voids. Evidence for such a shift in the halo mass function is given by Goldberg et al. (2004), who estimate the halo mass function of our void galaxy sample and find that the best-fit theoretical mass function has mass underdensity  $\delta = -0.6$ , similar to the underdensity in galaxies.

How do these results fit into the galaxy formation scenario? One possibility is that void galaxies have formed recently and are young, hence the young stellar ages, low masses and the active star formation. However, for galaxies to form in low density environments at all, they would have to form before the matter in the voids flowed out to the higher density regions. The relative blueness and active star formation of the void galaxies would be explained if the void galaxies consumed their gas supply at a slower rate than galaxies at higher density.

## 6. Conclusions

Using a sample of  $\sim 10^3$  void galaxies from the SDSS with density contrast  $\delta\rho/\rho < -0.6$ , we are able to examine the environmental dependence of spectral properties of galaxies in extremely

underdense regions.

We compare the equivalent widths of void and wall galaxies. Using this simple approach, we find that void galaxies have larger equivalent widths of  $H\alpha$ , [OII],  $H\beta$ , NII and [OIII]. This is the case regardless of distance to the galaxy, brightness and morphological type. This would suggest that void galaxies have undergone recent star formation.

Void galaxies also show weaker Balmer decrements, as measured by  $D_n(4000)$ , which indicates that the stellar population includes a higher fraction of O and B stars. Thus, the emission line widths and continuum shape yield evidence of enhanced star formation over a range of timescales.

Specific star-formation rates (estimated SFRs normalized by the stellar mass of the galaxy) of void galaxies are generally higher than for wall galaxies. Un-normalized SFRs are similar or slightly higher for wall galaxies than void galaxies, but the void galaxies tend to have smaller stellar masses.

These spectroscopic results corroborate the photometric evidence given by Rojas et al. (2004) that void galaxies are bluer than wall galaxies of similar luminosity and morphology.

Thus, we show that the trend of increasing SFR with decreasing density, seen heretofore in denser regions, does indeed continue into the rarefied environment of voids.

### Acknowledgments

Funding for the creation and distribution of the SDSS Archive has been provided by the Alfred P. Sloan Foundation, the Participating Institutions, the National Aeronautics and Space Administration, the National Science Foundation, the U.S. Department of Energy, the Japanese Monbukagakusho, and the Max Planck Society. The SDSS Web site is <http://www.sdss.org/>.

The SDSS is managed by the Astrophysical Research Consortium (ARC) for the Participating Institutions. The Participating Institutions are The University of Chicago, Fermilab, the Institute for Advanced Study, the Japan Participation Group, The Johns Hopkins University, Los Alamos National Laboratory, the Max-Planck-Institute for Astronomy (MPIA), the Max-Planck-Institute for Astrophysics (MPA), New Mexico State University, University of Pittsburgh, Princeton University, the United States Naval Observatory, and the University of Washington.

We thank Christy Tremonti and Andrew Hopkins for useful conversations and for assistance with the systematics in the SFR calculations. MSV acknowledges support from NSF grant AST-0071201 and a grant from the John Templeton Foundation.

### REFERENCES

Abazajian, K., et al. 2003, AJ, 126, 2081

- Abazajian, K., et al. 2004, *AJ*, 128, 502
- Balogh, M. L., Morris, S. L., Yee, H. K. C., Carlberg, R. G., & Ellingson, E. 1997, *ApJL*, 488, 75
- Balogh, M. L., Schade, D., Morris, S. L., Yee, H. K. C., Carlberg, R. G., & Ellingson, E. 1998, *ApJL*, 504, 75
- Balogh, M. L., Morris, S. L., Yee, H. K. C., Carlberg, R. G., & Ellingson, E. 1999, *ApJ*, 527, 54
- Balogh, M. L., Couch, W. J., Smail, I., Bower, R. G., & Glazebrook, K. 2002, *MNRAS*, 335, 10
- Balogh, M. L., et al. 2004, *MNRAS*, 348, 1355
- Benson, A. J., Hoyle, F., Torres, F., & Vogeley, M. S. 2003, *MNRAS*, 340, 160
- Blanton, M. R., et al. 2002, *ApJ*, 594, 186
- Bruzual, G. 1983, *ApJ*, 273, 105
- Couch, W. J. & Sharples, R. M. 1987, *MNRAS*, 229, 423
- Couch, W. J., Balogh, M. L., Bower, R. G., Smail, I., Glazebrook, K., & Taylor, M. 2001, *ApJ*, 549, 820
- da Costa, L. N., et al. 1998, *AJ*, 116, 1
- Dressler, A. 1980, *ApJ*, 236, 351
- Dressler, A., Thompson, I. B., & Shectman, S. 1985, *ApJ*, 288, 481
- Eisenstein, D. J., et al. 2001, *AJ*, 122, 2267
- Falco, E. E., et al. 1999, *PASP*, 111, 438
- Fukugita, M., Ichikawa, T., Gunn, J. E., Doi, M., Shimasaku, K., & Schneider, D. P. 1996, *AJ*, 111, 1748
- Goldberg, D. & Vogeley, M. S. 2004, *ApJ*, 605, 1
- Goldberg, D. M., Jones, T.D., Hoyle, F., Rojas, R. R., Vogeley, M. S. & Blanton, M.R. 2004, *ApJ*, submitted, astro-ph/0406527
- Gómez, P. L., et al. 2003, *ApJ*, 584, 210
- Grogin, N. A., & Geller, M. J. 1999, *ApJ*, 118, 2561
- Grogin, N. A., & Geller, M. J. 2000, *ApJ*, 119, 32
- Gunn, J. E. & Gott, J. R. I. 1972, *ApJ*, 176, 1
- Gunn, J. E., et al. 1998, *ApJ*, 116, 3040
- Hashimoto, Y., Oemler, A. J., Lin, H., & Tucker, D. L. 1998, *ApJ*, 499, 589
- Hopkins, A. M., et al. 2003, *ApJ*, 599, 971
- Hogg, D. W., Finkbeiner, D. P., Schlegel, D. J., & Gunn, J. E. 2001, *AJ*, 122, 2129
- Kauffmann, G. et al. 2003, *MNRAS*, 341, 33

- Kauffmann, G. et al. 2004, MNRAS, accepted, astro-ph/0402030
- Kennicutt, R. C. 1983, ApJ, 272, 54
- Kennicutt, R. C. Jr. 1992, ApJ, 388, 310
- Kennicutt, R. C., Jr. 1998, ARA&A, 36, 189
- Kennicutt, R. C. & Kent, S. M., 1983, AJ, 88, 1094
- Koo, D. C. & Kron, R. G. 1992 ARA&A30,613
- Lewis, I., et al. 2002, MNRAS, 334, 673
- Lupton, R. H., et al. 2002, in preparation
- Miller, N. A. & Owen, F. N. 2002, AJ, 124, 2453
- Pier, J. R., Munn, J. A., Hindsley, R. B., Hennessy, G. S., Kent, S. M., Lupton, R. H., & Ivezić, Ž. 2003, AJ, 125, 1559
- Poggianti, B. M., Smail, I., Dressler, A., Couch, W. J., Barger, A. J., Butcher, H., Ellis, R. S., & Oemler, A. J. 1999, ApJ, 518, 576
- Postman, M., & Geller, M. J. 1984, ApJ, 281, 95
- Rojas, R. R., Vogeley, M. S., Hoyle, F. & Brinkmann, J., 2004, ApJ, accepted (Dec. 10, 2004 issue), astro-ph/0307274
- Salpeter, E. E. 1955, ApJ, 121, 161
- Sérsic J. L. 1968, Atlas de Galaxias Australes. Observatorio Astronómico, Cordoba.
- Smith, J. A., et al. 2002, AJ, 123, 2121
- Solanes, J. M., Manrique, A., González-Casado, G., García-Gómez, C., Giovanelli, R., & Haynes, M. P. 2001, ApJ, 548, 97
- Stoughton, C. et al. 2002, AJ, 123, 485
- Strauss, M. A., et al. 2002, AJ, 124, 1810S
- Tanaka, M. et al. 2003, ApJ, submitted
- Tran, K. H., Simard, L., Zabludoff, A. I. & Mulchaey, J. S. 2001, ApJ, 549, 172
- York, D. G. et al. 2000, AJ, 120, 1579
- Zabludoff, A. I. & Mulchaey, J. S. 1998, ApJ, 496, 39

DISTANT SAMPLE				
Full ( $-22.5 \leq M_r \leq -17.77$ ) [ $N_V = 1010, N_W = 12732$ ]				
Property	Void (VGD) $\mu \pm \sigma_\mu$	Wall (WGD) $\mu \pm \sigma_\mu$	KS ( $P$ ) Probability	$[N_V, N_W]$
EW(H $\alpha$ ) [Å]	$19.14 \pm 0.680$	$11.77 \pm 0.158$	$< 10^{-4}$	(1005, 12636)
EW([OII]) [Å]	$14.26 \pm 0.395$	$9.441 \pm 0.093$	$< 10^{-4}$	(1006, 12301)
EW(H $\beta$ ) [Å]	$2.571 \pm 0.146$	$0.828 \pm 0.035$	$< 10^{-4}$	(997, 12544)
EW([NII]) [Å]	$6.553 \pm 0.181$	$5.065 \pm 0.049$	$< 10^{-4}$	(1006, 12586)
EW([OIII]) [Å]	$4.694 \pm 0.335$	$2.197 \pm 0.061$	$< 10^{-4}$	(994, 12373)
$D_n 4000$	$1.515 \pm 0.011$	$1.649 \pm 0.003$	$< 10^{-4}$	(714, 9862)
$\text{Log}_{10}(\text{Mass}/M_\odot)$	$10.13 \pm 0.015$	$10.43 \pm 0.004$	$< 10^{-4}$	(1010, 12732)
SFR(H $\alpha$ ) [ $M_\odot/\text{yr}$ ]	$0.734 \pm 0.025$	$0.747 \pm 0.007$	$< 10^{-4}$	(850, 8930)
SFR([OII]) [ $M_\odot/\text{yr}$ ]	$0.448 \pm 0.015$	$0.488 \pm 0.006$	$< 10^{-4}$	(841, 8764)
S-SFR(H $\alpha$ ) [ $\text{yr}^{-1}$ ]	$(3.744 \pm 0.108) \times 10^{-11}$	$(2.629 \pm 0.034) \times 10^{-11}$	$< 10^{-4}$	(850, 8930)
S-SFR([OII]) [ $\text{yr}^{-1}$ ]	$(4.892 \pm 0.890) \times 10^{-11}$	$(3.020 \pm 0.251) \times 10^{-11}$	$< 10^{-4}$	(841, 8764)
Bright ( $M_r \leq -19.5$ ) [ $N_V = 409, N_W = 7831$ ]				
Property	Void (VGD <sub>b</sub> ) $\mu \pm \sigma_\mu$	Wall (WGD <sub>b</sub> ) $\mu \pm \sigma_\mu$	KS ( $P$ ) Probability	$[N_V, N_W]$
EW(H $\alpha$ ) [Å]	$14.47 \pm 0.932$	$8.542 \pm 0.175$	$< 10^{-4}$	(406, 7774)
EW([OII]) [Å]	$9.338 \pm 0.429$	$6.884 \pm 0.089$	$< 10^{-4}$	(399, 7548)
EW(H $\beta$ ) [Å]	$1.246 \pm 0.201$	$0.018 \pm 0.038$	$< 10^{-4}$	(401, 7699)
EW([NII]) [Å]	$6.606 \pm 0.332$	$4.711 \pm 0.066$	$< 10^{-4}$	(407, 7743)
EW([OIII]) [Å]	$2.706 \pm 0.531$	$1.172 \pm 0.055$	$< 10^{-4}$	(401, 7574)
$D_n 4000$	$1.602 \pm 0.017$	$1.711 \pm 0.004$	$< 10^{-4}$	(287, 6069)
$\text{Log}_{10}(\text{Mass}/M_\odot)$	$10.52 \pm 0.016$	$10.70 \pm 0.004$	$< 10^{-4}$	(409, 7831)
SFR(H $\alpha$ ) [ $M_\odot/\text{yr}$ ]	$1.136 \pm 0.063$	$0.920 \pm 0.016$	$< 10^{-4}$	(306, 4956)
SFR([OII]) [ $M_\odot/\text{yr}$ ]	$0.736 \pm 0.051$	$0.626 \pm 0.013$	$< 10^{-4}$	(304, 4876)
S-SFR(H $\alpha$ ) [ $\text{yr}^{-1}$ ]	$(3.133 \pm 0.169) \times 10^{-11}$	$(2.137 \pm 0.004) \times 10^{-11}$	$< 10^{-4}$	(306, 4956)
S-SFR([OII]) [ $\text{yr}^{-1}$ ]	$(3.061 \pm 0.279) \times 10^{-11}$	$(2.192 \pm 0.053) \times 10^{-11}$	$< 10^{-4}$	(304, 4876)
Faint ( $M_r > -19.5$ ) [ $N_V = 601, N_W = 4901$ ]				
Property	Void (VGD <sub>f</sub> ) $\mu \pm \sigma_\mu$	Wall (WGD <sub>f</sub> ) $\mu \pm \sigma_\mu$	KS ( $P$ ) Probability	$[N_V, N_W]$
EW(H $\alpha$ ) [Å]	$22.31 \pm 0.929$	$16.93 \pm 0.287$	$< 10^{-4}$	(599, 4862)
EW([OII]) [Å]	$17.57 \pm 0.554$	$13.50 \pm 0.178$	$< 10^{-4}$	(593, 4753)
EW(H $\beta$ ) [Å]	$3.452 \pm 0.202$	$2.095 \pm 0.067$	$< 10^{-4}$	(531, 4334)
EW([NII]) [Å]	$6.517 \pm 0.204$	$5.630 \pm 0.074$	$< 10^{-4}$	(599, 4843)
EW([OIII]) [Å]	$6.038 \pm 0.423$	$3.817 \pm 0.128$	$< 10^{-4}$	(593, 4799)
$D_n 4000$	$1.456 \pm 0.013$	$1.551 \pm 0.004$	$< 10^{-4}$	(427, 3793)
$\text{Log}_{10}(\text{Mass}/M_\odot)$	$9.873 \pm 0.015$	$10.02 \pm 0.005$	$< 10^{-4}$	(601, 4901)
SFR(H $\alpha$ ) [ $M_\odot/\text{yr}$ ]	$0.508 \pm 0.0237$	$0.530 \pm 0.009$	0.0254	(544, 3974)
SFR([OII]) [ $M_\odot/\text{yr}$ ]	$0.286 \pm 0.017$	$0.316 \pm 0.007$	0.0298	(537, 3888)
S-SFR(H $\alpha$ ) [ $\text{yr}^{-1}$ ]	$(4.146 \pm 0.137) \times 10^{-11}$	$(3.349 \pm 0.005) \times 10^{-11}$	$< 10^{-4}$	(544, 3974)
S-SFR([OII]) [ $\text{yr}^{-1}$ ]	$(5.725 \pm 1.375) \times 10^{-11}$	$(4.058 \pm 0.147) \times 10^{-11}$	0.0034	(537, 3888)

Table 1: Means, errors on the means and KS test probabilities that the void and wall galaxies are drawn from the same parent population for the spectroscopic properties of void and wall galaxies in the distant sample ( $100 \leq r \leq 260h^{-1}\text{Mpc}$ ). The number of galaxies (void and wall) in each sample and sub-sample are listed next to the magnitude range heading as  $[N_V \text{ (void)}, N_W \text{ (wall)}]$ . Small values of  $P$  correspond to a low probability that the two samples are drawn from the same parent population. In this case, the KS test shows that the void and wall galaxies are drawn from different populations based on emission line EWs, stellar masses, H $\alpha$  and [OII] derived SFRs and S-SFRs, and  $D_n 4000$ . The differences between the means of the different parameters measured are on average  $> 5\sigma_\mu$ , except for the SFR(H $\alpha$ ) and SFR([OII]) in the faint sub-sample, where the difference is  $\sim 2\sigma_\mu$ . Void galaxies on average have higher S-SFRs, larger EWs, smaller stellar masses and smaller  $D_n 4000$ .

NEARBY SAMPLE				
Full ( $-19.9 \leq M_r \leq -14.5$ ) [ $N_V = 194, N_W = 2256$ ]				
Property	Void (VGD) $\mu \pm \sigma_\mu$	Wall (WGD) $\mu \pm \sigma_\mu$	KS ( $P$ ) Probability	$[N_V, N_W]$
EW(H $\alpha$ ) [Å]	35.31 $\pm$ 0.262	26.18 $\pm$ 0.645	0.0021	(187, 2202)
EW(H $\beta$ ) [Å]	7.317 $\pm$ 0.738	5.702 $\pm$ 0.242	0.0007	(192, 2226)
EW([NII]) [Å]	5.175 $\pm$ 0.338	4.298 $\pm$ 0.097	0.0611	(191, 2232)
EW([OIII]) [Å]	18.50 $\pm$ 2.111	14.17 $\pm$ 0.548	$< 10^{-4}$	(188, 2211)
$D_n4000$	1.261 $\pm$ 0.019	1.314 $\pm$ 0.005	$< 10^{-4}$	(119, 1545)
$\text{Log}_{10}(\text{Mass}/M_\odot)$	8.692 $\pm$ 0.060	8.803 $\pm$ 0.018	0.0592	(194, 2256)
SFR(H $\alpha$ ) [ $M_\odot/\text{yr}$ ]	0.162 $\pm$ 0.012	0.146 $\pm$ 0.006	0.3410	(183, 2020)
S-SFR(H $\alpha$ ) [ $\text{yr}^{-1}$ ]	$(25.55 \pm 0.353) \times 10^{-11}$	$(31.70 \pm 0.169) \times 10^{-11}$	0.0001	(182, 2005)
Bright ( $M_r \leq -17.0$ ) [ $N_V = 76, N_W = 1071$ ]				
Property	Void (VGD <sub>b</sub> ) $\mu \pm \sigma_\mu$	Wall (WGD <sub>b</sub> ) $\mu \pm \sigma_\mu$	KS ( $P$ ) Probability	$[N_V, N_W]$
EW(H $\alpha$ ) [Å]	33.316 $\pm$ 3.74	21.91 $\pm$ 0.809	0.0005	(76, 1060)
EW(H $\beta$ ) [Å]	5.939 $\pm$ 0.769	3.770 $\pm$ 0.210	0.0006	(76, 1055)
EW([NII]) [Å]	7.223 $\pm$ 0.733	5.203 $\pm$ 0.157	0.0034	(76, 1062)
EW([OIII]) [Å]	11.615 $\pm$ 2.41	8.276 $\pm$ 0.525	0.0133	(76, 1056)
$D_n4000$	1.287 $\pm$ 0.032	1.371 $\pm$ 0.008	$< 10^{-4}$	(50, 792)
$\text{Log}_{10}(\text{Mass}/M_\odot)$	9.333 $\pm$ 0.066	9.390 $\pm$ 0.018	0.4123	(76, 1071)
SFR(H $\alpha$ ) [ $M_\odot/\text{yr}$ ]	0.323 $\pm$ 0.048	0.194 $\pm$ 0.011	0.0009	(73, 933)
S-SFR(H $\alpha$ ) [ $\text{yr}^{-1}$ ]	$(17.57 \pm 3.222) \times 10^{-11}$	$(12.57 \pm 0.958) \times 10^{-11}$	$< 10^{-4}$	(73, 933)
Faint ( $M_r > -17.0$ ) [ $N_V = 118, N_W = 1185$ ]				
Property	Void (VGD <sub>f</sub> ) $\mu \pm \sigma_\mu$	Wall (WGD <sub>f</sub> ) $\mu \pm \sigma_\mu$	KS ( $P$ ) Probability	$[N_V, N_W]$
EW(H $\alpha$ ) [Å]	36.68 $\pm$ 3.60	30.14 $\pm$ 0.977	0.3740	(111, 1142)
EW(H $\beta$ ) [Å]	8.220 $\pm$ 1.111	7.443 $\pm$ 0.412	0.2920	(116, 1171)
EW([NII]) [Å]	3.821 $\pm$ 0.378	3.477 $\pm$ 0.121	0.4446	(115, 1170)
EW([OIII]) [Å]	23.17 $\pm$ 3.073	19.55 $\pm$ 0.905	0.0481	(112, 1155)
$D_n4000$	1.243 $\pm$ 0.022	1.253 $\pm$ 0.007	$< 10^{-4}$	(69, 753)
$\text{Log}_{10}(\text{Mass}/M_\odot)$	8.279 $\pm$ 0.060	8.273 $\pm$ 0.019	0.3589	(118, 1185)
SFR(H $\alpha$ ) [ $M_\odot/\text{yr}$ ]	0.054 $\pm$ 0.006	0.098 $\pm$ 0.005	0.1725	(109, 1066)
S-SFR(H $\alpha$ ) [ $\text{yr}^{-1}$ ]	$(29.19 \pm 4.527) \times 10^{-11}$	$(46.37 \pm 2.713) \times 10^{-11}$	0.0269	(109, 1066)

Table 2: Means, errors on the means and KS test probabilities that the void and wall galaxies are drawn from the same parent population for the spectroscopic properties of void and wall galaxies in the nearby sample ( $r < 72h^{-1}\text{Mpc}$ ). The number of galaxies (void and wall) in each sample and sub-sample are listed next to the magnitude range heading as  $[N_V \text{ (void), } N_W \text{ (wall)}]$ . Small values of  $P$  correspond to a low probability that the two samples are drawn from the same parent population. The KS test shows that void galaxies appear to have stronger emission line EWs than wall galaxies in all cases. The average difference between the means of the EWs and  $D_n4000$ s is about  $2\sigma_\mu$ . However, the SFRs and stellar masses are not significantly different. Only the bright void galaxy sub-sample shows a larger S-SFR(H $\alpha$ ) than wall galaxies.



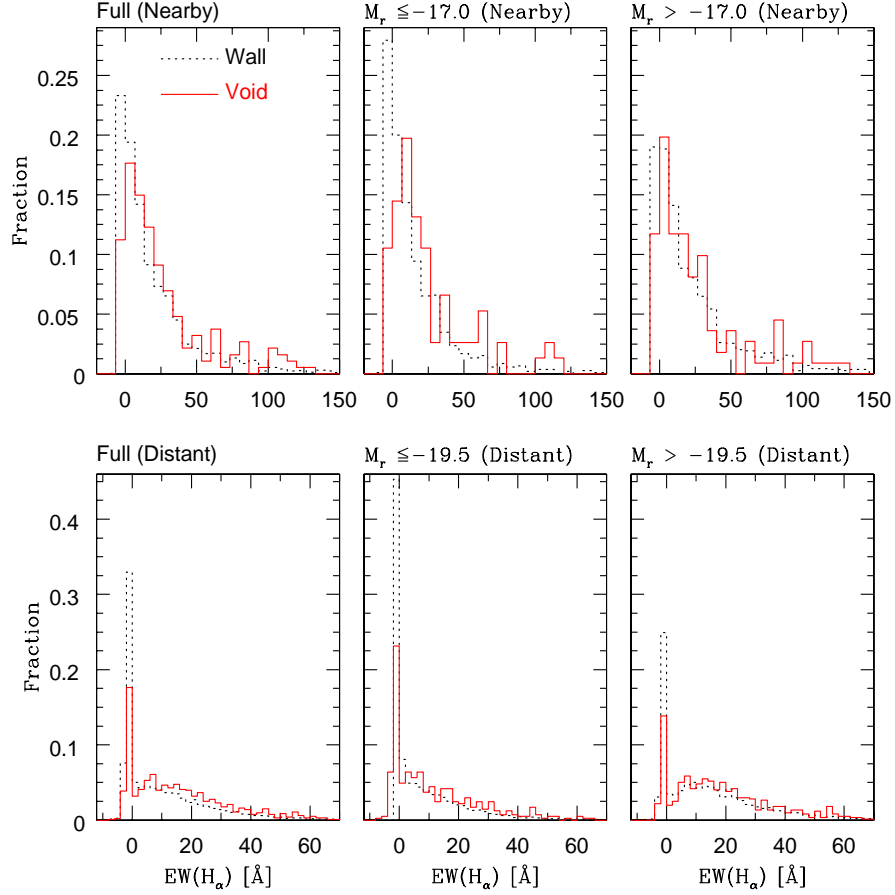


Fig. 1.— Distribution of  $H\alpha$  equivalent widths. We show the normalized fraction of void (solid lines) and wall galaxies (dotted lines) as a function of  $EW(H\alpha)$ . The top row shows the results for the nearby ( $r < 72h^{-1}\text{Mpc}$ ) galaxies, the bottom row shows the results for the distant ( $100 \leq r \leq 260h^{-1}\text{Mpc}$ ) galaxies. The first, second and third columns are the full, bright and faint samples. The fraction of galaxies per  $6.5\text{\AA}$  (nearby) and  $2\text{\AA}$  (distant) bin of  $EW(H\alpha)$  is shown on the Y-axis. The KS statistic reveals that the distant void galaxy (bright, faint, and full) and respective wall galaxy samples are very different from one another, with a probability of  $< 0.01\%$  that they are drawn from the same parent population. In the case of the nearby galaxies, only the faint galaxy distributions (top right panel) have a higher probability ( $P \lesssim 0.37$ ) of being similar.

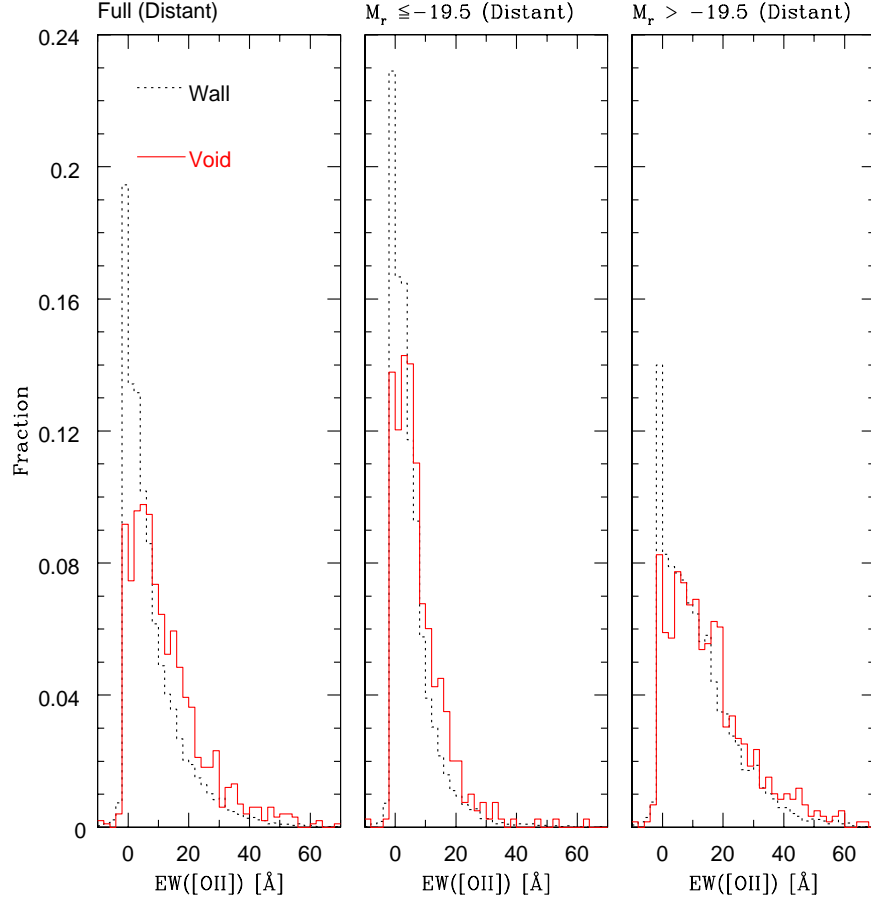


Fig. 2.— Distribution of [OII] equivalent widths. We show the normalized fraction of void (solid lines) and wall galaxies (dotted lines) as a function of  $\text{EW}([\text{OII}])$ . The first, second and third columns are the full, bright and faint distant samples. The fraction of galaxies per  $2\text{\AA}$  bin of  $\text{EW}([\text{OII}])$  is shown on the Y-axis. The KS statistic reveals that the distant void galaxy (bright, faint, and full) and respective wall galaxy samples are very different from one another, with a probability of  $< 0.01\%$  that they are drawn from the same parent population.

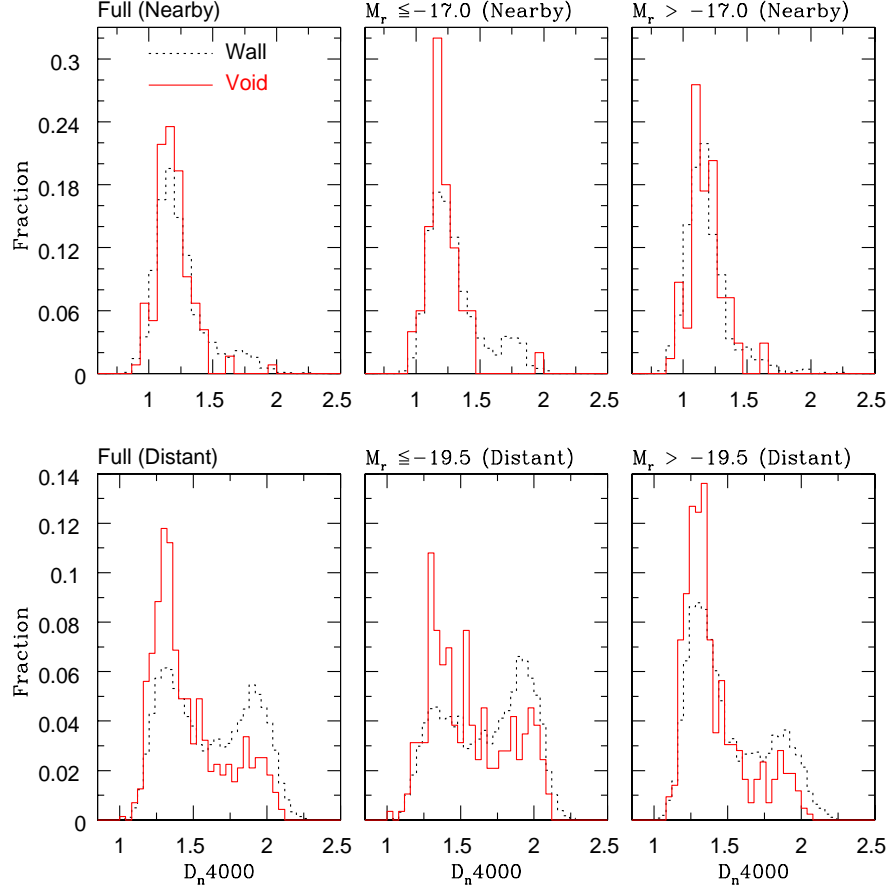


Fig. 3.— Distribution of the 4000 Å Balmer break. We show the normalized fraction of void (solid lines) and wall galaxies (dotted lines) as a function of  $D_{n4000}$ . The top row shows the results for the nearby ( $r < 72h^{-1}\text{Mpc}$ ) galaxies, the bottom row shows the results for the distant ( $100 \leq r \leq 260h^{-1}\text{Mpc}$ ) galaxies. The first, second and third columns are the full, bright and faint samples. The fraction of galaxies per 0.067 (nearby) and 0.04 (distant) bin of  $D_{n4000}$  is shown on the Y-axis. The KS statistic reveals that the distant and nearby void galaxy (bright, faint, and full) and respective wall galaxy samples are very different from one another, with a probability of  $< 0.01\%$  that they are drawn from the same parent population.

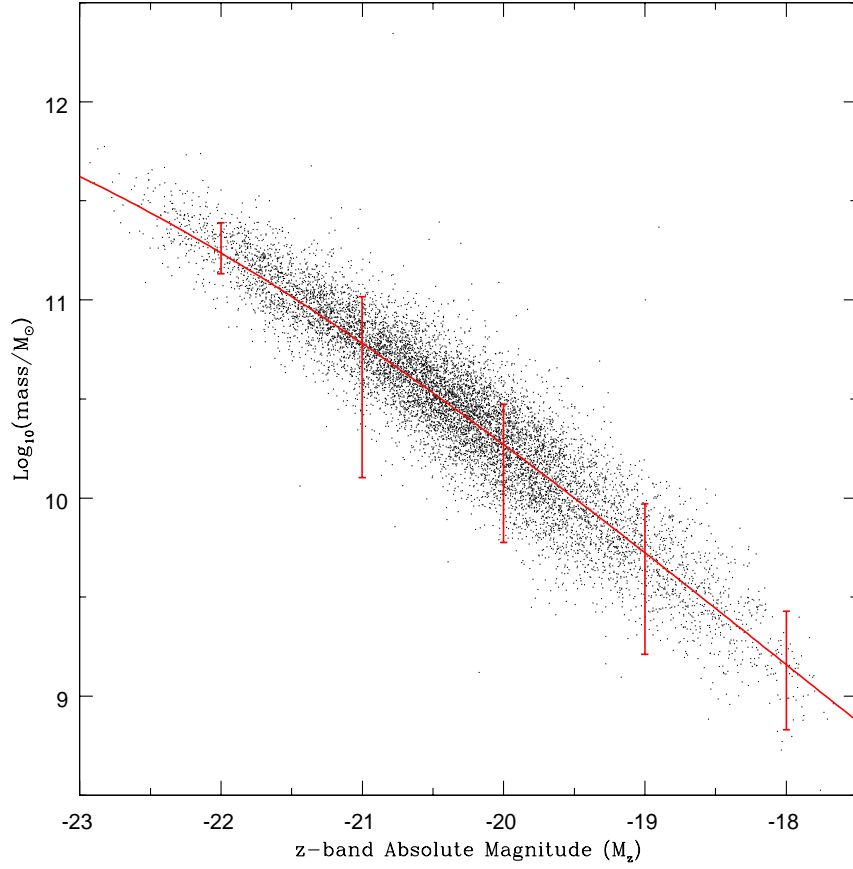


Fig. 4.— Plot of  $\text{Log}_{10}(\text{Mass}/M_{\odot})$  vs.  $z$ -band absolute magnitude using Kauffmann’s et al (2003) stellar masses (points). Error bars are the  $1\sigma$  errors of stellar masses in bins  $\Delta M_z = 1$  wide. The solid line is a least squares fit. We use this linear fit to estimate the stellar masses of other galaxies in our sample using their  $z$ -band flux.

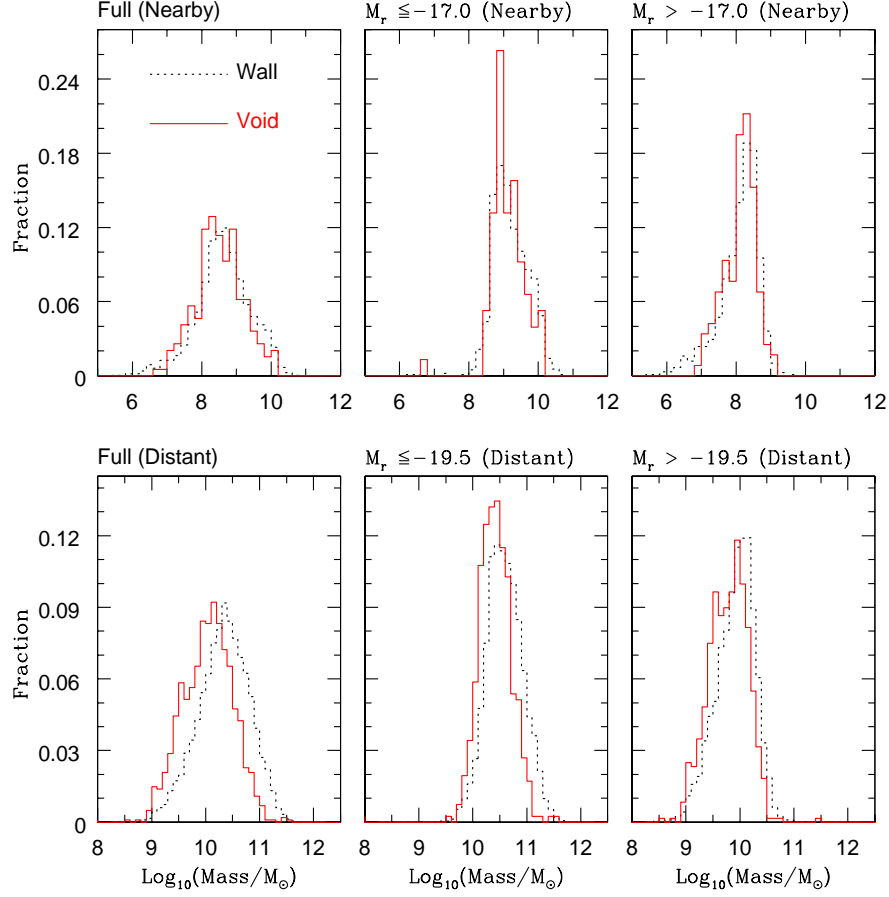


Fig. 5.— Stellar Mass Distribution. We show the normalized fraction of void (solid lines) and wall galaxies (dotted lines) as a function of  $\text{Log}_{10}(\text{Mass}/M_{\odot})$ . The top row shows the results for the nearby ( $r < 72h^{-1}\text{Mpc}$ ) galaxies, the bottom row shows the results for the distant ( $100 \leq r \leq 260h^{-1}\text{Mpc}$ ) galaxies. The first, second and third columns are the full, bright and faint samples. The fraction of galaxies per  $5M_{\odot}$  (nearby) and  $10M_{\odot}$  (distant) bin of  $\text{Log}_{10}(\text{Mass}/M_{\odot})$  is shown on the Y-axis. The KS statistic reveals that the distant void galaxy (bright, faint, and full) and respective wall galaxy samples are very different from one another, with a probability of  $< 0.01\%$  that they are drawn from the same parent population. In the case of the nearby galaxies, only the bright galaxy distributions have a higher probability ( $P \lesssim 0.36$ ) of being similar.

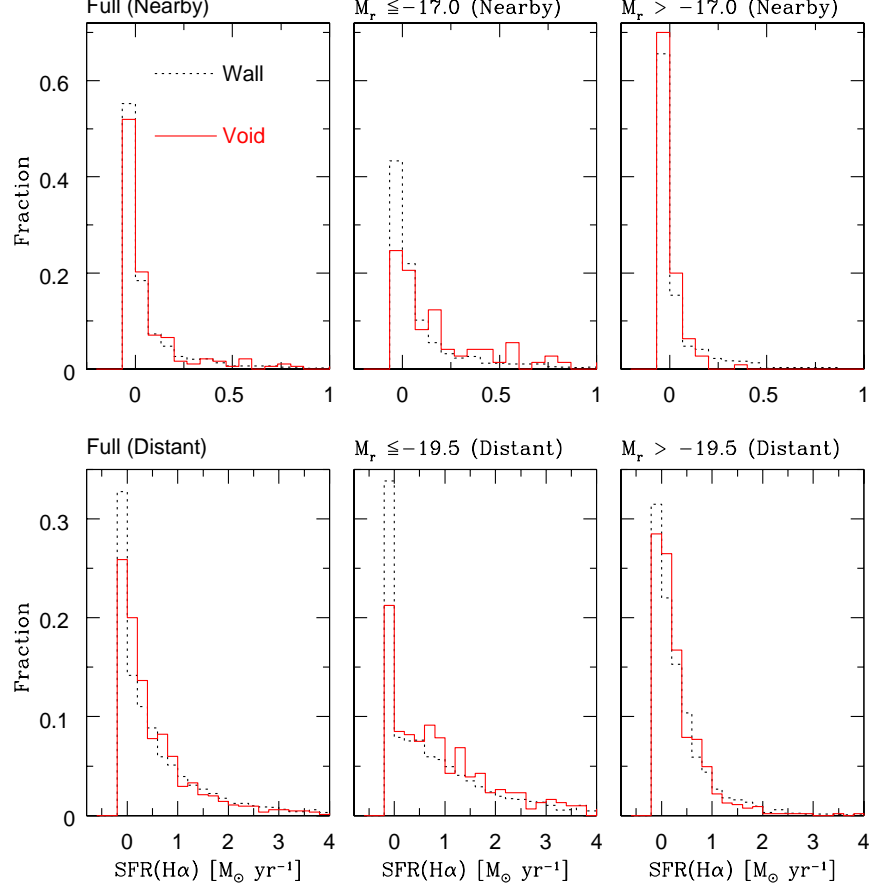


Fig. 6.— Distribution of  $H\alpha$  star formation rates. We show the normalized fraction of void (solid lines) and wall galaxies (dotted lines) as a function of  $SFR(H\alpha)$ . The top row shows the results for the nearby ( $r < 72h^{-1}\text{Mpc}$ ) galaxies, the bottom row shows the results for the distant ( $100 \leq r \leq 260h^{-1}\text{Mpc}$ ) galaxies. The first, second and third columns are the full, bright and faint samples. The fraction of galaxies per  $0.067M_{\odot}\text{yr}^{-1}$  bin of  $SFR(H\alpha)$  is shown on the Y-axis. The KS statistic reveals that the distant void galaxy (bright and full) and respective wall galaxy samples are very different from one another, with a probability of  $< 0.01\%$  that they are drawn from the same parent population.

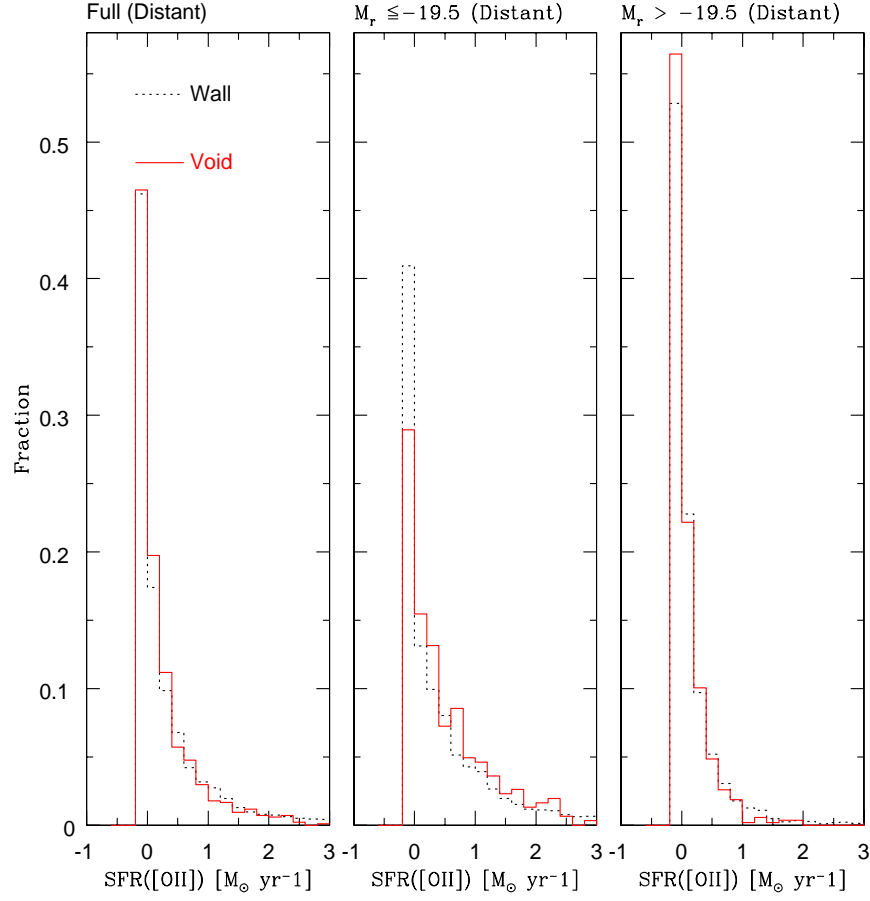


Fig. 7.— Distribution of [OII] star formation rates. We show the normalized fraction of void (solid lines) and wall galaxies (dotted lines) as a function of  $\text{SFR}([\text{OII}])$ . The first, second and third columns are the full, bright and faint distant samples. The fraction of galaxies per  $0.067 M_{\odot} \text{ yr}^{-1}$  bin of  $\text{SFR}([\text{OII}])$  is shown on the Y-axis. The KS statistic reveals that the distant void galaxy (bright and full) and respective wall galaxy samples are very different from one another, with a probability of  $< 0.01\%$  that they are drawn from the same parent population.

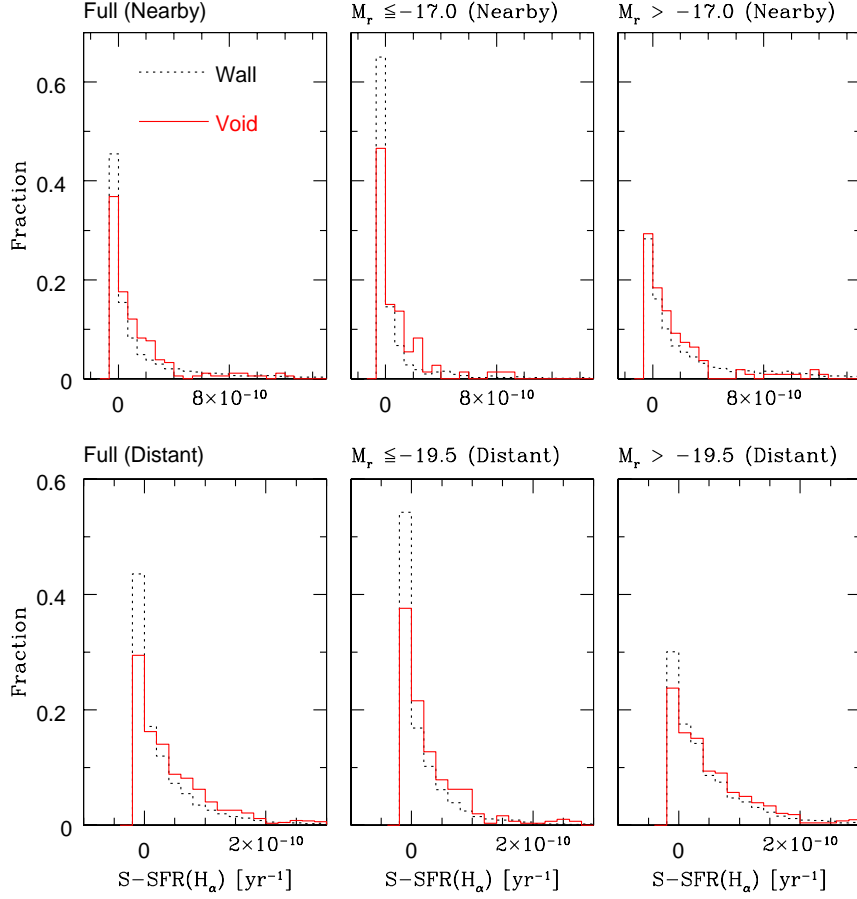


Fig. 8.— Distribution  $H\alpha$  specific star formation rates. We show the normalized fraction of void (solid lines) and wall galaxies (dotted lines) as a function of  $S\text{-SFR}(H\alpha)$ . The top row shows the results for the nearby ( $r < 72h^{-1}\text{Mpc}$ ) galaxies, the bottom row shows the results for the distant ( $100 \leq r \leq 260h^{-1}\text{Mpc}$ ) galaxies. The first, second and third columns are the full, bright and faint samples. The fraction of galaxies per  $10^{-10}\text{yr}^{-1}$  bin of  $S\text{-SFR}(H\alpha)$  is shown on the Y-axis. The KS statistic reveals that the distant void galaxy (bright, faint, and full) and respective wall galaxy samples are very different from one another, with a probability of  $< 0.01\%$  that they are drawn from the same parent population. In the case of the nearby galaxies, only the bright galaxy distributions have a higher probability ( $P \lesssim 0.027$ ) of being similar.



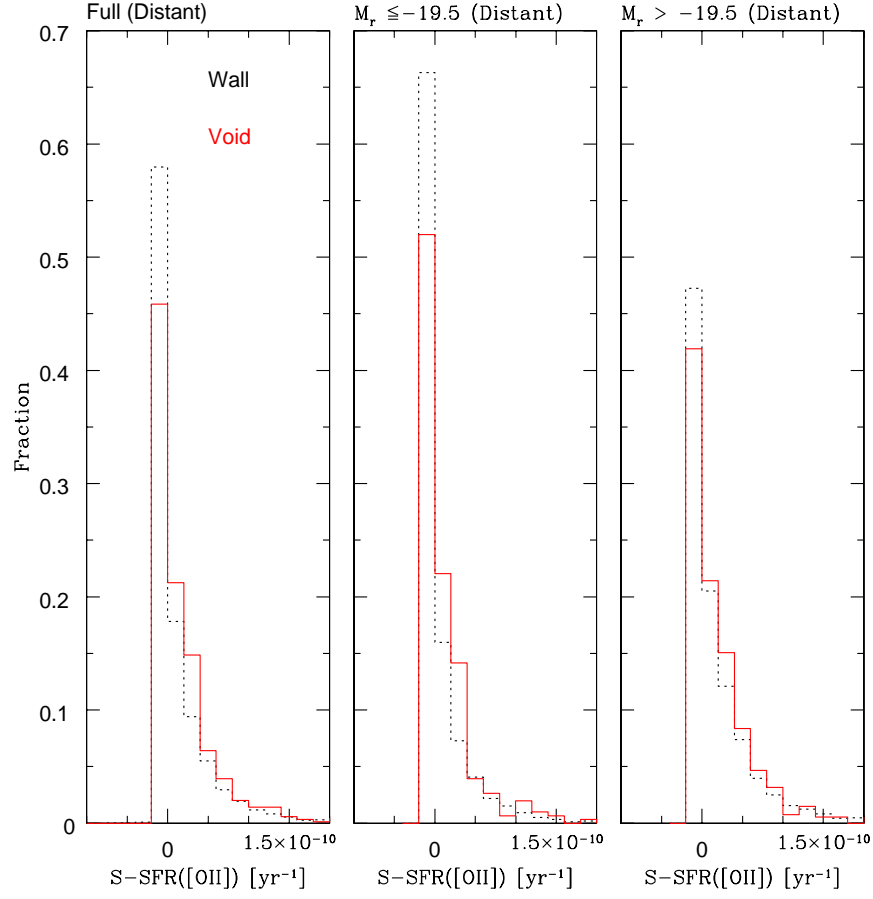


Fig. 9.— Distribution of [OII] specific star formation rates. We show the normalized fraction of void (solid lines) and wall galaxies (dotted lines) as a function of  $S-SFR([OII])$ . The first, second and third columns are the full, bright and faint distant samples. The fraction of galaxies per  $10^{-10} \text{yr}^{-1} \text{bin}$  of  $SFR([OII])$  is shown on the Y-axis. The KS statistic reveals that the distant void galaxy (bright, faint, and full) and respective wall galaxy samples are very different from one another, with a probability of  $< 0.034\%$  that they are drawn from the same parent population.